

Contents lists available at ScienceDirect

Chemical Geology

journal homepage: www.elsevier.com/locate/chemgeo



Perennial flow through convergent hillslopes explains chemodynamic solute behavior in a shale headwater catchment



Elizabeth M. Herndon^{a,*}, Grit Steinhoefel^b, Ashlee L.D. Dere^c, Pamela L. Sullivan^d

- ^a Department of Geology, 221 McGilvrey Hall, Department of Geology, Kent State University, Kent, OH 44240, United States
- ^b Alfred Wegener Institute, Helmholtz Centre for Polar and Marine Research, Bremerhaven, Germany
- ^c Department of Geography/Geology, University of Nebraska Omaha, Omaha, NE, United States
- d Department of Geography and Atmospheric Science, University of Kansas, Lawrence, KS, United States

ARTICLE INFO

Editor: J. Gaillardet

Keywords:
Concentration-discharge behavior
Interflow
Colloids
Surface-groundwater interactions
Metals

ABSTRACT

Stream chemistry reflects the mixture of complex biogeochemical reactions that vary across space and time within watersheds. For example, streams experience changing hydrologic connectivity to heterogeneous water sources under different flow regimes; however, it remains unclear how seasonal flow paths link these different sources and regulate concentration-discharge behavior, i.e., changes in stream solute concentration as a function of discharge. At the Susquehanna Shale Hills Critical Zone Observatory (SSHCZO) in central Pennsylvania, USA, concentrations of chemostatic solutes (K, Mg, Na, Si, Cl) vary little across a wide range of discharge values while concentrations of chemodynamic solutes (Fe, Mn, Ca) decrease sharply with increasing stream discharge. To elucidate controls on chemodynamic solute behavior, we investigated the chemistry of surface water and shallow subsurface water at the SSHCZO in early autumn when discharge was negligible and concentrations of chemodynamic solutes were high. Dissolved ions, colloids, and micron-sized particles were extracted from hillslope soils and stream sediments to evaluate how elements were mobilized into pore waters and transported from hillslopes to the stream.

During the study period when flow was intermittent, the stream consisted of isolated puddles that were chemically variable along the length of the channel. Inputs of subsurface water to the stream were limited to an area of upwelling near the stream headwaters, and the water table remained over a meter below the stream bed along the rest of the channel. Chemodynamic elements Fe and Mn were preferentially mobilized from organic-rich soils as a mixture of dissolved ions, colloids, and micron-sized particles; consequently, subsurface water draining organic-rich soils in the upper catchment was enriched in Fe and Mn. Conversely, Ca increased towards the catchment outlet and was primarily mobilized from stream sediments as Ca²⁺. Concentrations of chemostatic solutes were relatively invariable throughout the catchment.

We conclude that chemodynamic behavior at SSHCZO is driven by seasonally variable connectivity between the stream and hillslope soils. During the dry season, stream water derives from a shallow perched water table (interflow) that upwells to generate metal-rich stream headwaters. High concentrations of soluble Fe and Mn at low discharge occur when metal-rich headwaters are flushed to the catchment outlet during periodic rain events. Interflow during the dry season originates from water that infiltrates through organic-rich swales; thus, metals in the stream at low flow are ultimately derived from convergent hillslopes where biological processes have concentrated and/or mobilized these chemodynamic elements. In contrast, high concentrations of Ca²⁺ at low discharge are likely mobilized from stream sediments that contain secondary calcite precipitates. We infer that chemodynamic solutes are diluted at high discharge primarily due to increased flow through planar hillslopes. This study highlights how spatially heterogeneous biogeochemistry and seasonally variable flow paths regulate concentration-discharge behavior within catchments.

1. Introduction

Element concentrations in streams vary with stream discharge in

patterns that integrate watershed processes over varying spatial and temporal scales. Chemostatic behavior occurs when solute concentrations vary only slightly as stream discharge increases by orders of

E-mail address: eherndo1@kent.edu (E.M. Herndon).

^{*} Corresponding author.

magnitude, as commonly observed for products of rock weathering (Godsey et al., 2009). Such invariant concentrations are attributed to mixing of concentrated solute pools with dilute rainwater, increases in mineral weathering during rain events, and rapid equilibration between minerals and infiltrating water (Godsey et al., 2009; Maher, 2011; Ameli et al., 2017; Li et al., 2017). Chemodynamic behavior occurs when solute concentrations either increase (enrichment) or decrease (dilution) with increasing discharge (e.g., Johnson et al., 1969; Kirchner, 2003). These patterns are attributed to varying inputs of chemically distinct water sources (e.g., groundwater vs. soil water, seasonally variable tributary mixing) (Bishop et al., 2004; Herndon et al., 2015a; Baronas et al., 2017; Hoagland et al., 2017; Torres et al., 2017), differential mobilization of dissolved versus colloidal and particulate phases (Trostle et al., 2016; McIntosh et al., 2017), or rapid depletion of weatherable minerals during rain events (Li et al., 2017). Increasingly, chemodynamic solutes are identified as having non-linear log-log concentration-discharge patterns that reflect multiple processes under different flow regimes (Moatar et al., 2017; Zhang, 2017). Evaluating hydrologic and biogeochemical processes that control concentration-discharge patterns may enable better understanding of watershed dynamics and prediction of solute loadings and chemical denudation. Though much research has focused on perennial streams, it is necessary to investigate concentration-discharge behavior in intermittent and ephemeral streams given that they comprise a majority of stream length in headwater catchments of the United States (Nadeau and Rains, 2007).

Previous research at the Susquehanna Shale Hills Critical Zone Observatory (SSHCZO) in central Pennsylvania identified chemostatic solutes (e.g., K, Na, Mg, Si, Cl) whose concentrations vary little across a wide range of discharge values and chemodynamic solutes (e.g., Ca, Fe, Mn, Al, dissolved organic carbon) whose concentrations decrease sharply with increasing discharge in the stream (Fig. 1) (Herndon et al., 2015a). Concentrations of chemodynamic solutes are correlated with dissolved organic carbon (DOC) in organic-rich pore waters that may serve as primary sources of organic and metal solutes to the stream during summer and fall flushing events (Andrews et al., 2011). Solutes associated with DOC were termed "bioactive" due to either intense biotic cycling and storage in plant biomass (Ca, Mn) or complexation by DOC released during organic matter decomposition (Fe, Al) (Herndon et al., 2015a; Herndon et al., 2015b). As a result, chemodynamic solute concentrations in the stream were proposed to be controlled by changing hydrologic connectivity of the stream to organic-rich soils under different flow regimes. In contrast, solutes that are not correlated with DOC (Na, Mg, K, Si, Cl) are spatially homogeneous across organic-rich and organic-poor soils and chemostatic in the streams. Chemostasis at SSHCZO is driven by hydrogeochemical processes in the soil that include mixing of dilute rain water with concentrated pore waters (e.g., Cl) and increased clay dissolution (e.g., Mg) during rain events (Li et al., 2017).

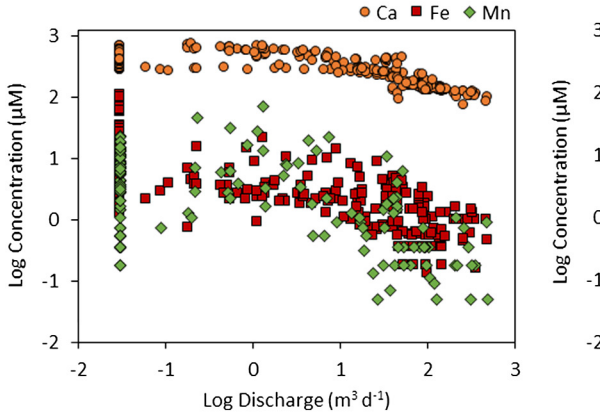
However, it remains unclear how elements are mobilized from hillslopes and transported to the stream along these variable flow paths. The purpose of this study was to investigate sources of the chemodynamic solutes Fe, Mn, and Ca to the stream by exploring hydrologic connectivity between hillslopes and the stream under low to no flow conditions when chemodynamic solute concentrations were high. We also investigated the potential for metals and organic matter to be mobilized from soil into stream water as dissolved ions, colloids, and micron-sized particles. Solutes that are operationally defined as passing through a 0.45 µm filter consist of both colloids and dissolved ions (Aiken et al., 2011), while particles, which do not pass through a $0.45\,\mu m$ filter, are also mobilized from soils and can dominate removal of poorly soluble elements such as Fe, Al, and Ti (Jin et al., 2010; Yesavage et al., 2012; Bern and Yesavage, 2018). Elements that are mobilized from soils can undergo dissolution, precipitation, and sorption reactions along flow paths before reaching the stream, which influence the residence time and bioavailability of elements within catchments (Kim et al., 2017). Identifying linkages between hydrologic connectivity and chemical reactions that occur along flow paths is essential for deconstructing the processes that underlie concentrationdischarge patterns.

2. Methods

2.1. Susquehanna Shale Hills critical zone observatory

The Susquehanna Shale Hills Critical Zone Observatory (SSHCZO) is a $0.8\,\mathrm{km}^2$ first-order catchment located in central Pennsylvania, U.S.A., within the Ridge and Valley Province of the Appalachian Mountains. This forested, V-shaped catchment is oriented in an east-west direction and is drained by a westward flowing stream that experiences intermittent flow during the dry season from late summer to early autumn (Fig. 2). Elevation of the ground surface ranges from 310 m at the eastern high point to 256 m at the catchment outlet (Lin et al., 2006). North- and south-facing slopes are generally steep (up to 25–48%), planar, and dominated by thin (< 0.5 m depth of augerable regolith) and well-drained soils. Seven swales located along the hillslopes contain thick (1–3 m depth) colluvial soils that remain relatively wet throughout the year (Lin et al., 2006; Qu and Duffy, 2007).

The SSHCZO is underlain almost entirely by Silurian Rose Hill Shale with increasing occurrence of thin sandstone and limestone interbeds in



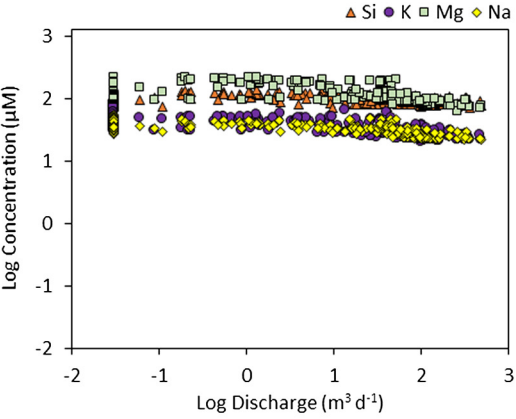


Fig. 1. Log C (solute concentration; μ mol L^{-1}) versus log Q (discharge; $m^3 d^{-1}$) of chemodynamic elements Ca, Fe, and Mn (*left panel*) and chemostatic elements Si, K, Mg, and Na (*right panel*) in the Susquehanna Shale Hills CZO. Chemostatic elements are defined as having log-C/log-Q slopes between -0.1 and 0.1, while chemodynamic elements are defined as having log-C/log-Q slopes either < 0.1 (dilution behavior) or > 0.1 (enrichment behavior). All chemostatic elements here exhibit dilution behavior. Data reported in Herndon et al. (2015a).

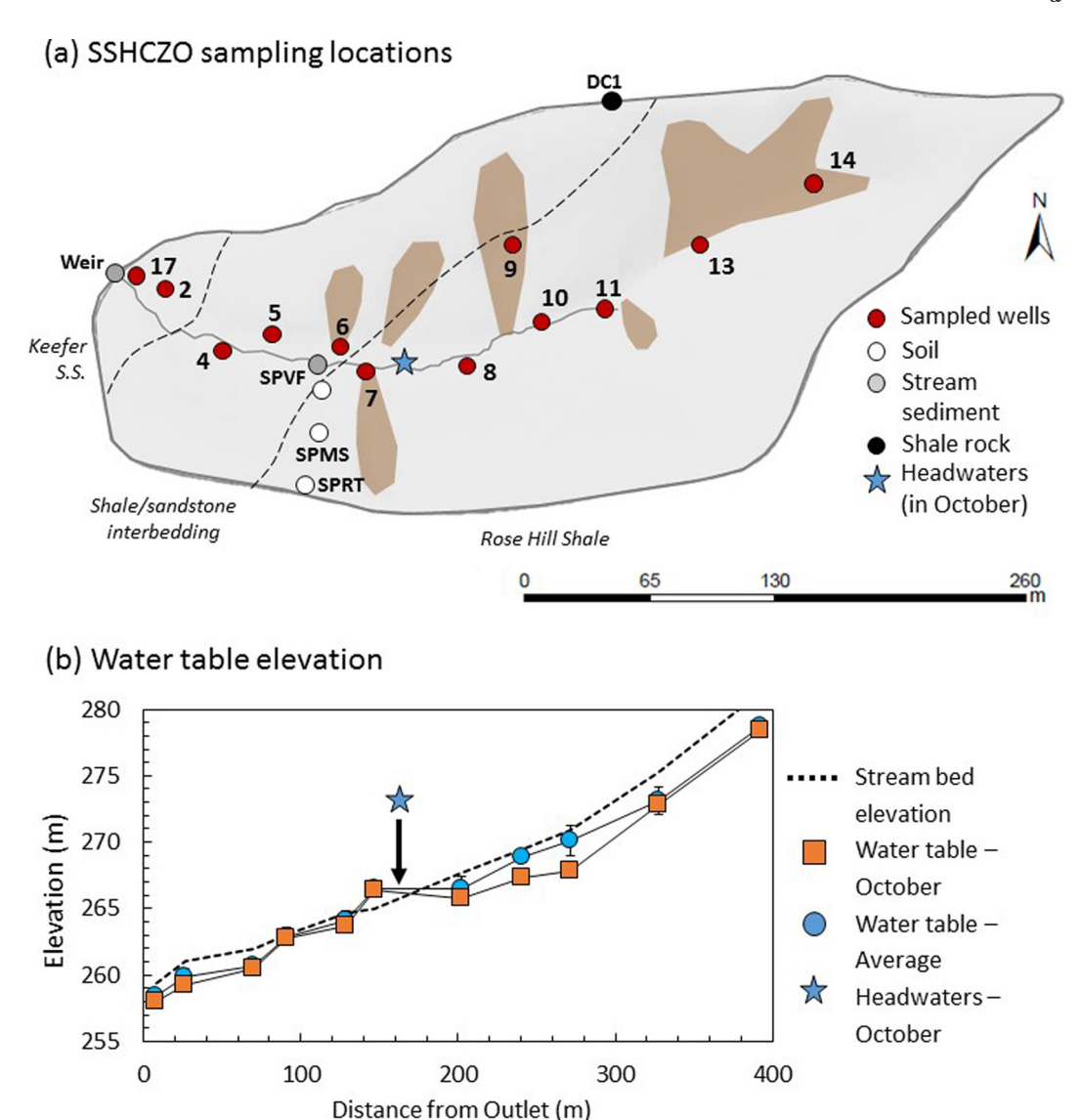


Fig. 2. (a) Map of the Susquehanna Shale Hills Critical Zone Observatory with sampled wells indicated by numbered red symbols and locations of soil (SPRT, SPMS, SPVF), stream sediment (Weir, SPVF) and bedrock (DC1) samples indicated by white, grey, and black symbols, respectively. Convergent hillslopes (swales) are shown as areas of brown overlay on the map. The position of the stream is indicated by the solid line running through the map center, with the position of the headwaters during the October sampling period marked with a blue star. Positions of lithologic boundaries are marked with dashed lines. (b) Water table elevation (m) measured in groundwater wells in early October 2014 (orange squares) was similar to or lower than average values of groundwater level measured monthly between December 2012 through March 2014 (blue filled cycles) (Sullivan et al., 2016a). The water table was consistently below the stream bed (dashed line) except for well 7. The water table measured in well 9 in a swale (not shown) was > 4 m below land surface. The position of the headwaters shown in (a) is indicated by the blue star. (For interpretation of the references to color in this figure legend, the reader is referred to the web version of this article.)

the western section that grade into a contact with the Keefer sandstone near the outlet (Fig. 2). The Rose Hill Shale is an organic-poor grey shale dominated by quartz and clay minerals (illite, chlorite, and vermiculite) with minor amounts of plagioclase feldspar, pyrite, and carbonates (Jin et al., 2010). Pyrite and primary carbonates are depleted to > 15-20 m below the ridges and > 2-8 m below the stream bed, roughly coincident with the water table, while secondary calcite precipitates in the valley floor (Brantley et al., 2013; Jin et al., 2014; Sullivan et al., 2016a). Shale weathering produces acidic, residual soils that are depleted of major elements (e.g., K, Mg, Fe, Al) due to solute and particle loss that occur during weathering of illite and chlorite minerals (Jin et al., 2010). Surface soils are enriched with Mn and other contaminant metals (e.g., Pb, Cd, Zn) due to atmospheric deposition from regional industry and biological cycling through vegetation (Herndon et al., 2011; Ma et al., 2014; Herndon et al., 2015b; Kraepiel et al., 2015).

Mean annual temperature and precipitation were 10 °C and $102\,\mathrm{cm}\,\mathrm{y}^{-1}$ respectively for the 30-year period of record from 1985 to 2015 (USC00368449; NOAA, 2017). Precipitation that falls on the catchment infiltrates soil and flows laterally downslope through macropores and along soil horizon interfaces (Lin et al., 2006). Lateral flow ("interflow") comprises > 70% of stream flow with smaller contributions from surface runoff and deep groundwater (Li et al., 2017). This shallow interflow moves seasonally along permeable boundaries in the augerable regolith and permanently through fractured shale bedrock below the augerable regolith and recharges the stream in the valley floor. Permanent interflow mixes with the deeper regional water table periodically during the wet season (November - May) (Sullivan et al., 2016a). Approximately 40-50% of precipitation exits the catchment as stream discharge at the weir with 50-60% lost to the atmosphere through evapotranspiration and ~4% possibly exiting in deeper flow paths (Qu and Duffy, 2007; Herndon et al., 2015b; Li et al., 2017).

Stream flow decreases in the late summer and early autumn dry season when evapotranspiration is high.

2.2. Water sampling and chemical analysis

Synoptic sampling of surface water and well water during the dry season was used to identify connections between the surface and shallow subsurface flow paths that may have been obscured during higher flow conditions. Surface water and well water were collected from the SSHCZO catchment in mid-October 2014 during a dry period when stream flow was intermittent. The stream headwaters, defined as the furthest upstream pool of surface water, was located just above the lithologic contact between shale and sandstone-interbedded shale during the period of sampling (Fig. 2). No surface water existed in the channel upstream of this point, although it is important to note that ephemeral stream headwaters are reported by others to be further upcatchment (near well 11) during spring snow melt and storm events (e.g., Jin et al., 2014; Meek et al., 2016; Sullivan et al., 2016a). Downstream of the perennial headwaters as defined by this study, surface water was present in disconnected shallow puddles with no flow. Water was pooled in the stream bed above the weir but did not visibly flow out of the catchment during sampling.

Electrical conductivity (μ S cm $^{-1}$), temperature (°C), and pH were measured directly in the surface water. Water was pulled from surface puddles using an acid-washed plastic syringe, then filtered ($<0.45\,\mu$ m nylon syringe filter) into separate bottles for analysis of filterable cations (stored in plastic bottles and acidified with 2–3 drops ultrapure concentrated nitric acid), anions (stored in plastic bottles and not acidified), and dissolved organic carbon (stored in combusted glass vials and acidified with 2–3 drops ultrapure concentrated hydrochloric acid). Syringes were rinsed with the next water sample between each use.

Well water was sampled from 11 wells along the valley floor and one well on the south-facing hillslope (well 9) (Fig. 2). All wells were drilled to a depth of \sim 4 m below land surface (mbls), cased to \sim 3 mbls with PVC, and screened over the bottom ~1 m. Hydraulic conductivity (K) values were previous determined by slug tests using the Hvorslev's method and ranged over three orders of magnitude (1.41×10^{-8}) to $1.04 \times 10^{-5} \,\mathrm{m\,s^{-1}}$) with largest values observed in wells near the outlet (Table 2). Depth to the water table, measured as the difference between the height of the well casing and the level of water within the well, was recorded using a water table meter and later converted to absolute elevation (m). A multiparameter water quality meter (YSI Professional Series) was used to record pH and electrical conductivity directly in the well. A peristaltic pump with polyethylene tubing was used to purge each well before extracting water and filtering it through a $0.45\,\mu m$ polyethersulfone high capacity filter (Millipore). Subsamples for cation, anion, and DOC analyses were collected as described for surface waters.

Concentrations of filterable elements (Na, K, Ca, Mg, Fe, Mn) were quantified by inductively coupled plasma optical emission spectrophotometry (Optima 8000 ICP-OES). Concentrations of ferrous iron [Fe (II)] were determined using the 1,10-phenanthroline method. Briefly, aliquots of HCl-acidified water were reacted with the colorimetric indicator 1,10-phenanthroline (Hach Ferrous Iron Reagent Powder Pillows) and the resulting absorbance at 520 nm was measured using an spectrophotometer ultraviolet-visible (Shimadzu Absorbance was converted to concentration using calibration curves constructed from standard solutions of ferrous ammonium sulfate. Anion concentrations (F⁻, Cl⁻, Br⁻, NO₃⁻, SO₄²⁻, PO₄³⁻) were quantified by ion chromatography (ThermoFisher Dionex ICS-2100 with AS11-HC column). Dissolved organic carbon concentrations were quantified by combustion catalytic oxidation method (Shimadzu TOC-L). Specific ultraviolet absorbance (SUVA $_{254}$; L mg-C $^{-1}$ m $^{-1}$), reported as sample absorbance at 254 nm normalized to DOC concentration, was used as a proxy for the aromaticity of DOC (Weishaar et al., 2003).

SUVA₂₅₄ values were corrected for potential interference from high dissolved Fe concentrations following Weishaar et al. (2003).

2.3. Soil sampling and analysis

Hillslope soils were collected in approximately 10 cm depth increments from the ridge (SPRT), midslope (SPMS), and valley floor (SPVF) positions of the south planar transect (Fig. 2). Shale bedrock was collected above the carbonate weathering front at 1.1–1.2 m (DC1-8) and 6.1–6.3 m (DC1-26) depth below the soil surface. Soil and bedrock samples were ground to pass through a 100-mesh sieve. Bulk chemistry and mineralogy for these samples has been reported elsewhere (Jin et al., 2010). Shallow stream sediments (< 30 cm) were augured in October 2014 from midstream near well 8 and from near the catchment outlet above the weir. Stream sediments were homogenized, air-dried, then powdered to silt-sized particles in a high energy ball mill with a tungsten carbide vial set (Spex Mixer/Mill 8000 M).

To obtain water-extractable elements, powdered solids (~0.5 g) were extracted with 20 mL of room-temperature Milli-Q water for 30 min on a mechanical rotator (Bern et al., 2015). Slurries were centrifuged for 30 min at 4000 $\times g$ to pelletize particles but leave colloids and dissolved ions in the supernatant. Extract solutions were passed through 0.22 µm nylon and 10 kDa regenerated cellulose filters (Amicon Ultra-15) to obtain filtered (dissolved ions + colloids) and ultrafiltered (dissolved ions only) fractions, respectively. The 10 kDa filters were rinsed five times prior to use by passing Milli-Q water (18 $M\Omega$) through the filter cartridge during centrifugation. Suspended grains extracted from the SPMS 0-10 cm soil were captured on the nylon filter ($> 0.22 \,\mu m$) and examined using scanning electron microscopy (see below). Filtered soil extracts were acidified with 2-3 drops of ultrapure 15 M HNO₃ prior to elemental analysis (Al, Ca, Fe, Mn, P, Ti, K, Mg) by ICP-OES. Elements K and Mg were only measured for SPMS and SPVF samples. Method blanks consisting of filtered Milli-O water were below detection for all elements except Al. The Al concentration in the filtered blank comprised between 12 and 100% of Al concentrations in filtered soil extracts and was subtracted out. Colloid concentrations were calculated as the difference in element concentrations measured in $< 0.22\,\mu m$ and $< 10\,kDa$ filtrates. Concentrations of solutes and colloids are reported per mass dry soil (μ mol kg⁻¹).

Hot-water extractable organic carbon (HWEOC) was collected from soils and sediments in order to quantify and characterize labile organic matter (Ghani et al., 2003). HWEOC (mg C g-soil⁻¹) was obtained by extracting residual material from the colloid extraction with 20 mL of heated Milli-Q water. Centrifuge tubes containing the water-soil slurry were placed in an oven at 80 °C for 16 h with occasional mixing. Slurries were then centrifuged for 30 min at 4000 \times g, and supernatant solutions were filtered ($< 0.22 \, \mu m$ nylon) and acidified with 2–3 drops ultrapure concentrated hydrochloric acid. Concentrations of dissolved organic carbon in hot-water extracts were quantified by combustion catalytic oxidation method. HWEOC absorbance from 190 to 800 nm was measured by UV-Visible spectroscopy (Agilent Cary 8454) and used to calculate SUVA₂₅₄ values (Weishaar et al., 2003). The concentration of DOC mobilized during colloid extraction (water soluble C; WSC) (Ghani et al., 2003) was quantified in a subset of < 0.22 µm filtrate solutions acidified with 2-3 drops ultrapure 12 M HCl. WSC concentrations were similar to HWEOC concentrations for tested soils, indicating that approximately half of the labile organic C was mobilized during colloid extraction. Concentrations of DOC in 0.45 µm filtered Milli-Q water were below detection ($< 1 \text{ mg L}^{-1}$), while DOC could not be quantified in ultrafiltrate solutions due to contamination from the cellulose filter.

2.4. Scanning electron microscopy

Scanning electron microscopy with energy dispersive x-ray spectroscopy (SEM-EDS; Hitachi TM3030 Tabletop Microscope) was used to examine particles mobilized from a surface soil by water-extraction

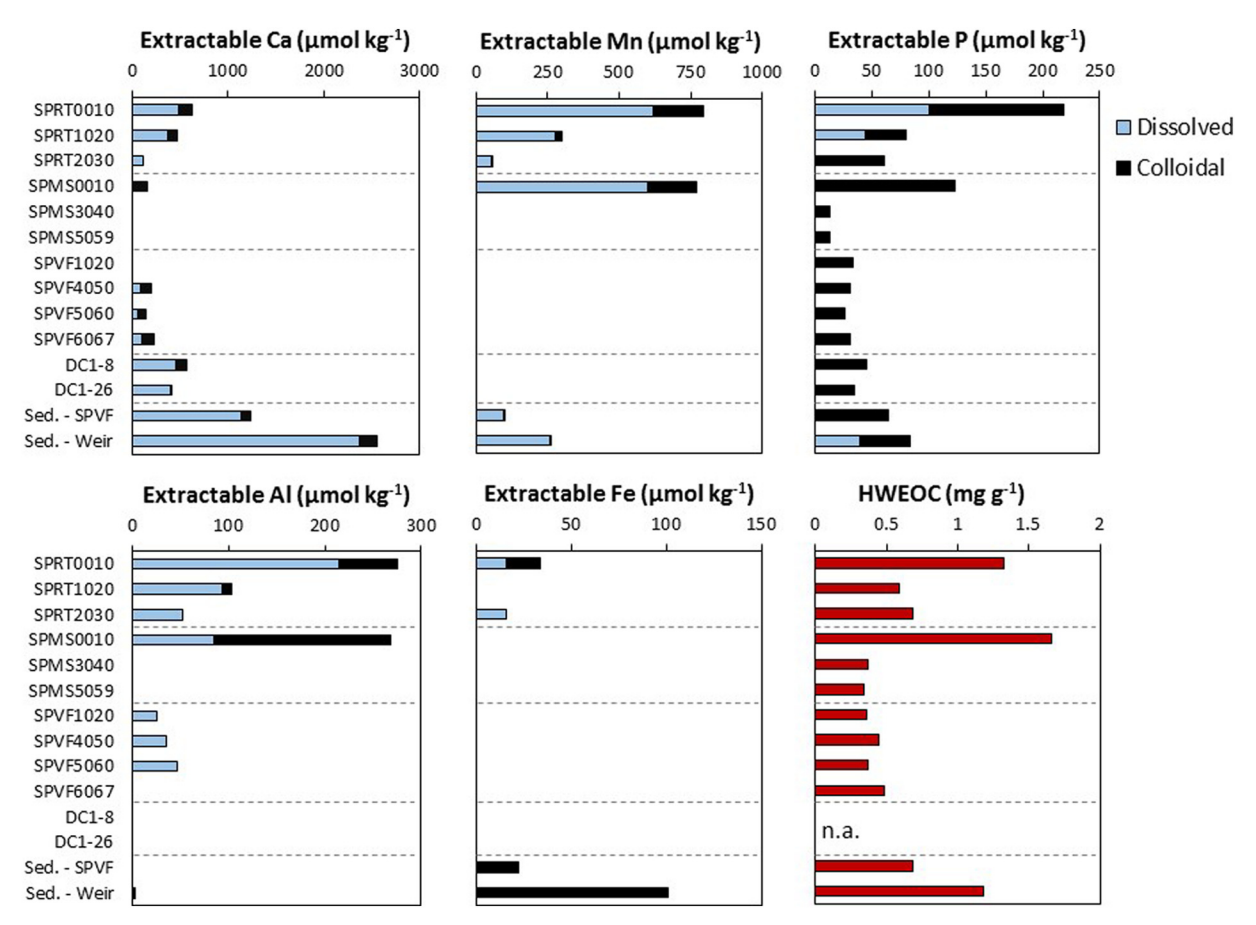


Fig. 3. Concentrations (μ mol kg $^{-1}$) of water-extractable dissolved (< 10 kDa) and colloidal (10 kDa – 0.22 μ m) elements and hot-water extractable organic C (HWEOC; mg g $^{-1}$) extracted from soils on a planar hillslope, shale bedrock (DC1-8 and DC1-26), and stream sediments (Sed. SPVF and Sed. Weir). The total length of each bar represents the sum of dissolved and colloidal phases.

("mobile particles") and reddish-black precipitates that formed in filtered, non-acidified water from well 8 during storage under oxic conditions. Backscattered electron images were used to evaluate particle morphology. Element mapping and single point measurements were used to quantify element abundance and element ratios.

3. Results

3.1. Soil and sediment geochemistry

Water-soluble elements extracted from soils and sediments were partitioned into dissolved ($<10\,kDa)$ and colloidal (10 kDa – 0.45 $\mu m)$ phases. Manganese, Ca, K, and Al were primarily mobilized as dissolved ions whereas Fe and P were mobilized as colloids (Fig. 3; Table 1). Concentrations of dissolved Mn²⁺ were high in organic-rich surface soils and sediments (up to 618 µmol kg⁻¹) but below detection in deeper mineral soils and shale bedrock (< 15 µmol kg⁻¹). Colloidal Mn comprised $\sim 22\%$ (=170 \pm 4 μ mol kg⁻¹) of Mn mobilized from shallow soils but < 8% ($< 25 \,\mu\text{mol kg}^{-1}$) of Mn mobilized from deeper soils and stream sediments. Concentrations of dissolved Ca²⁺ were high in stream sediments (=1760 \pm 620 μ mol kg⁻¹) relative to soils (< 480 μmol kg⁻¹) or shale bedrock collected above the carbonate weathering front (= $425 \pm 32 \,\mu\text{mol kg}^{-1}$), while concentrations of colloidal Ca were uniformly low (< 180 µmol kg⁻¹). Concentrations of dissolved K⁺ (ranging from 740 to 2360 µmol kg⁻¹) were consistently higher than colloidal K (140-503 µmol kg⁻¹). Both dissolved $(\leq 214 \,\mu\mathrm{mol\,kg^{-1}})$ and colloidal Al $(\leq 184 \,\mu\mathrm{mol\,kg^{-1}})$ were high in shallow soil but below detection with depth.

In contrast, Fe and P were primarily measured in the colloidal

fraction. Concentrations of dissolved Fe were low or below detection in all samples ($\leq \! 16\, \mu mol\, kg^{-1}$), and only colloidal Fe (range from 18 to $101\, \mu mol\, kg^{-1}$) was mobilized from stream sediment. Colloidal P comprised > 50% of mobile P in all samples and was highest in surface soils (120 $\pm 2\, \mu mol\, kg^{-1}$), while dissolved P was detected only in the ridge soil and stream sediment. Titanium and Mg were below detection in both the dissolved and colloidal fractions for all samples.

Hot-water extractable organic carbon (HWEOC) was high in organic-rich surface soils (> 1 mg g-soil $^{-1}$) relative to deeper organic-poor soils (< 0.7 mg g $^{-1}$) (Fig. 4; Table 1). SUVA $_{254}$ values for HWEOC decreased with depth within each soil profile. For stream sediments, HWEOC concentrations (0.7–1.2 mg g-soil $^{-1}$) and SUVA $_{254}$ values (1.0–1.2 L mg-C $^{-1}$ m $^{-1}$) were intermediate between shallow and deep soils. In comparison, stream water (2.7 \pm 1.2 L mg-C $^{-1}$ m $^{-1}$) and subsurface water (4.3 \pm 1.7 L mg-C $^{-1}$ m $^{-1}$) exhibited higher and more variable SUVA $_{254}$.

Particles mobilized from a surface soil (SPMS 0–10 cm) and analyzed by SEM-EDS were fine-grained ($<10\,\mu m$ diameter) and composed primarily of Si, Al, Ti, and Fe (Fig. 5a). Grains containing both Al and Si exhibited Al to Si ratios (1:1) consistent with the aluminosilicate mineral kaolinite, Al₂Si₂O₅(OH)₄, that forms in these soils during feldspar and vermiculite weathering (Jin et al., 2010). Iron and Ti were present in discrete particles that did not contain high concentrations of other elements and were presumably iron oxyhydroxides and titanium oxides. Particles with high Si/Al ratios (> 4) were interpreted to be small quartz grains.

Filtered, non-acidified water collected from well 8 developed reddish-black precipitates upon oxygenation during storage in a plastic bottle. These precipitates were evaluated as potential oxidation

Table 1 Element concentrations (μ mol kg⁻¹) in < 0.22 μ m and < 10 kDa water-soluble fractions extracted from soils (SPRT, SPMS, SPVF), shale bedrock (DC1-8 and DC1-26), and stream sediments (Sed. SPVF and Sed. Weir).

Sample	Depth (cm)	LOI ^a	HWEOC	HWEOC SUVA ₂₅₄	Water-extractable elements $< 0.22\mu m$ fraction $(\mu molkg^{-1})$					Water-extractable elements $< 10 kDa$ fraction (µmol kg $^{-1}$)				
		%	${\rm mgg^{-1}}$	$\mathrm{Lmg^{-1}m^{-1}}$	Al^b	Ca	Fe	Mn	P	Al	Ca	Fe	Mn	P
SPRT0010	5	15.3	1.33	1.11	276	624	34	793	218	214	477	16	618	100
SPRT1020	15	11.3	0.59	1.03	103	466	15	300	79	93	365	8	276	44
SPRT2030	25	7.66	0.68	0.61	< DL	110	< DL	59	60	52°	114	16	55	< DL
SPMS0010	5	12.6	1.66	1.94	268	160	< DL	769	123	84	< DL	< DL	601	< DL
SPMS3040	35	7.22	0.37	1.33	< DL	< DL	< DL	< DL	< DL	< DL	< DL	< DL	< DL	< DL
SPMS5059	54.5	7.01	0.34	1.40	< DL	< DL	< DL	< DL	< DL	< DL	< DL	< DL	< DL	< DL
SPVF1020	15	7.51	0.36	1.42	27	< DL	< DL	< DL	34	25	< DL	< DL	< DL	< DL
SPVF4050	45	7.53	0.44	1.25	51	193	< DL	< DL	31	34	87	< DL	< DL	< DL
SPVF5060	55	7.25	0.37	1.34	47	138	< DL	< DL	25	47	52	< DL	< DL	< DL
SPVF6067	63.5	6.84	0.49	1.29	47	221	< DL	< DL	31	< DL	104	< DL	< DL	< DL
DC1-8		6.13	n.a.	n.a.	< DL	572	< DL	11	45	< DL	457	< DL	10	< DL
DC1-26		5.84	n.a.	n.a.	< DL	403	< DL	5	35	< DL	392	< DL	5	< DL
Sed SPVF			0.69	0.96	< DL	1230	22	102	64	< DL	1139	< DL	97	< DL
Sed Weir			1.18	1.24	18	2554	101	261	84	< DL	2375	< DL	259	39
Analytical S	Analytical Std. Err.		0.01		7	6	3	2	7	7	6	3	2	7
Detection li	mit ^d		0.04		30	20	14	15	26	30	20	14	15	26

^a LOI = Loss-on-ignition at 550 °C.

products that form when reducing interflow upwells to the stream bed and/or mixes with oxygenated groundwater in the subsurface. Precipitates were large ($\sim 500 \, \mu m$), uniform, and composed primarily of Mn and Fe, presumably oxides, and enriched in C and P (Fig. 5b). Other rock-derived elements (Mg, Al, Si, K, Ca, Ti) within the particles were below the detection limits of the instrument ($< 1.0 \, wt\%$).

3.2. Surface and subsurface water chemistry

The water table measured in well 7 just upstream of the lithologic boundary was above the stream bed at the time of sampling and remained above the stream bed throughout the year with minimal seasonal fluctuation (Table 2; Fig. S1). In comparison, depth to the water table was 0.2 to 3.1 m below land surface (bls) along the rest of the channel and 4.3 m bls on the north hillslope (well 9) in October 2014 (Fig. 2b). These results were consistent with water table positions previously observed during the dry season (August–October) (Sullivan et al., 2016a). Based on these water table measurements, we defined an area of upwelling as the zone around well 7 between wells 6 and 8,

which was coincident with the location of the puddle defined as the stream headwaters in this study.

Given that water levels only suggest a potential for flow direction, we analyzed the chemistry of surface water and subsurface (well) water along the length of the channel to evaluate hydrologic connectivity. Solute concentrations reported for surface and subsurface water include all material that passed through a 0.45 µm filter. Surface water was chemically variable along the length of the channel (Fig. 6; Table 3). Concentrations of Fe and Mn were high near the headwaters $(26.7 \pm 3.0 \text{ and } 34.8 \pm 3.2 \,\mu\text{mol}\,\text{L}^{-1}, \text{ respectively})$ and decreased downstream (< 1 and $< 4 \mu mol L^{-1}$). For comparison, previous studies report consistently low Fe and Mn concentrations (< 2 and < 8 μmol L⁻¹) along the length of the flowing stream in spring (April–May) and late autumn (November) (Jin et al., 2014; Sullivan et al., 2016a). Conductivity (109 \pm 27 μ S cm⁻¹) increased towards the outlet and was higher than the annual average (62 μS cm⁻¹; Sullivan et al., 2016a). Concentrations of Ca²⁺ increased by a factor of three from the headwaters to the outlet, while Mg $^{2+}$, Na $^+$, and K $^+$ varied by less than a factor of two. Major anions SO $_4^{2-}$ and Cl $^-$ increased by 2–3× from

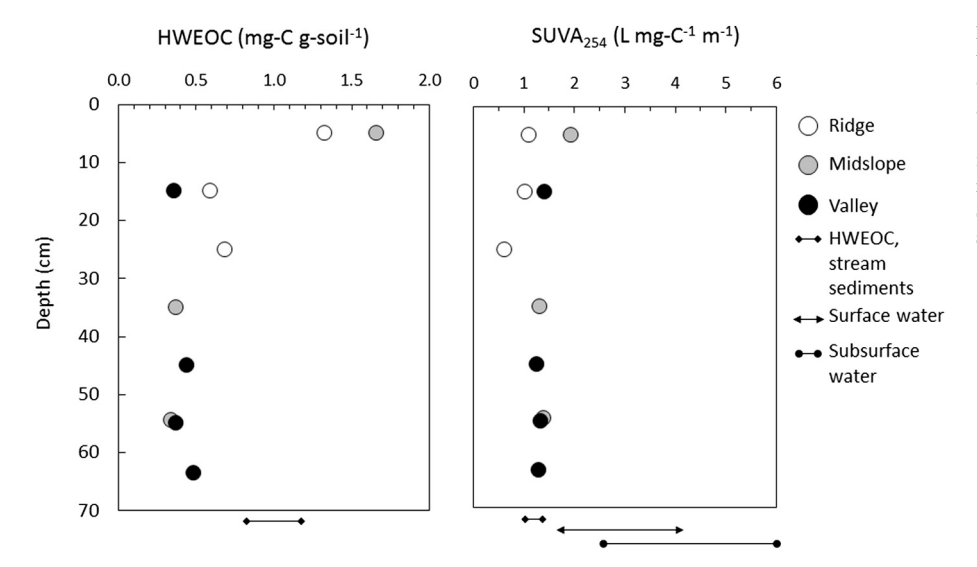


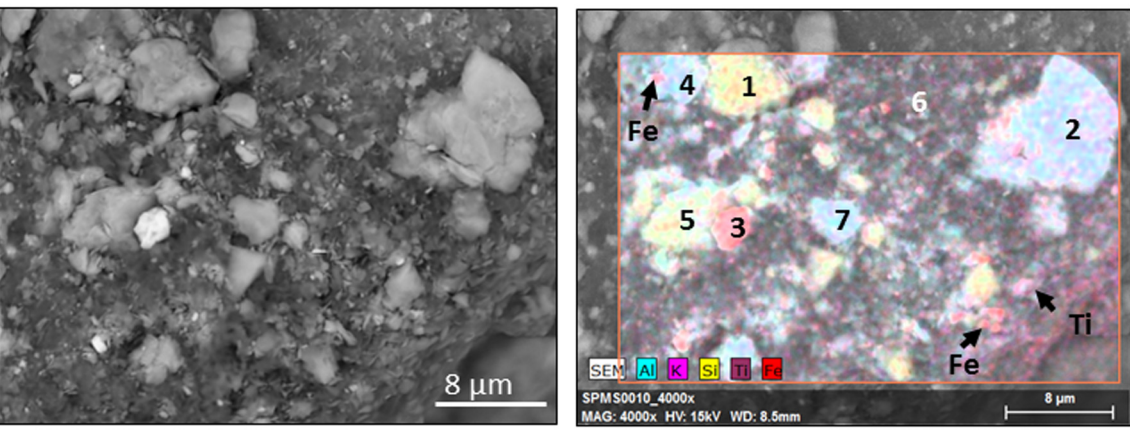
Fig. 4. Concentration (mg-C g-soil $^{-1}$) and specific ultraviolet absorption at 254 nm (SUVA $_{254}$; L mg-C $^{-1}$ m $^{-1}$) of hot-water extractable organic carbon as a function of depth in ridge (SPRT), midslope (SPMS), and valley floor (SPVF) soils. For comparison, arrows indicate the range of HWEOC values measured in stream sediments, and the range of SUVA $_{254}$ values measured for surface water, subsurface water, and HWEOC from stream sediments.

 $^{^{}b}$ Al concentrations in $< 0.22\,\mu m$ filtrate are blank-corrected; All other elements were < DL in blanks.

 $^{^{\}rm c}$ Concentration in < 10 kDa filtrate exceeded < 0.22 μm filtrate.

^d Detection limits converted from solution (μ mol L⁻¹) to soil concentrations (μ mol kg⁻¹).

(a) SPMS 0-10 cm, water-extractable particles



(b) Precipitate formed during oxidation of subsurface water (well 8)

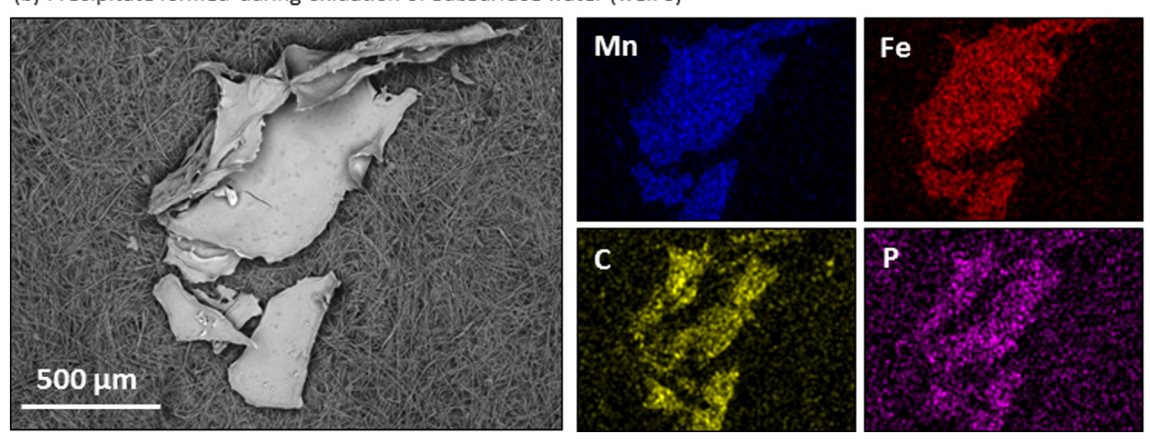


Fig. 5. (a) (left) Backscattered electron image of particles mobilized during colloid extraction and captured on a 0.45 μ m nylon filter. (right) Color overlay on backscattered electron image showing distribution of Al (blue), K (pink) Si (yellow), Ti (purple), and Fe (red). Individual grains were identified as quartz (grains 1 and 5), kaolinite (2, 4, and 7) and Fe oxide-coated kaolinite (3). Identification was based on Al-normalized element stoichiometry (atm. %) for quartz (Si/Al > 5) and kaolinite (Si/Al = 1), with high Fe indicting Fe oxide. The filter background (area #6) was > 93% C and O. (b) Backscattered image (left) and associated elemental maps (right) of a precipitate that formed in subsurface water (well 8) following collection and filtration through a 0.7 μ m glass fiber filter. (For interpretation of the references to color in this figure legend, the reader is referred to the web version of this article.)

Table 2Water table elevations measured during this study (October 2014) and averaged over the year^a.

aged over the year.												
Site ID	Distance from outlet (m)	Ground elevation (m)	Water table elev. (Oct. 12, 2014) (m)	Water table elev. (average) (m)	Hydraulic conductivity (m s ⁻¹)							
Well 17	8.00	259.4	258.0	258.5	1.08×10^{-6}							
Well 2	26.47	261.1	259.2	259.9	1.04×10^{-5}							
Well 4	70.32	261.9	260.5	260.7	4.23×10^{-7}							
Well 5	91.01	263.0	262.8	262.9	1.24×10^{-6}							
Well 6	128.98	264.6	263.7	264.1	1.51×10^{-7}							
Well 7	147.11	265.0	266.4	266.5	2.50×10^{-6}							
Well 8	202.08	267.7	265.8	266.5	9.81×10^{-7}							
Well 9	219.78	277.2	272.9	273.4	n.a.							
Well 10	240.43	269.4	267.3	268.9	6.98×10^{-7}							
Well 11	271.16	270.9	267.8	270.1	2.09×10^{-7}							
Well 13	327.21	275.3	272.9	273.1	1.80×10^{-7}							
Well 14	392.2	281.3	278.4	278.7	1.41×10^{-8}							

^a Sullivan et al., 2016b.

headwaters to outlet, while DOC concentrations (1660 $\pm~110\,\mu mol\,L^{-1})$ were variable along the stream. Stream pH was circumneutral (6.8 $\pm~0.3)$ with little variability.

Subsurface water from the upper, eastern portion of the catchment contained high concentrations of Fe (as Fe²⁺) and Mn but low concentrations of Ca relative to subsurface water from the lower, western portion of the catchment (Fig. 6; Table 3). Concentrations of Fe and Mn in the upper wells (wells 7, 8, 9, 10, 11, and 13) were 2 to 60 times higher than their annual average concentrations (Fig. 7). The highest concentrations of Fe (98 μ mol L⁻¹) and Mn (53 μ mol L⁻¹) were measured in well 9, which drains a swale on the north hillslope. In contrast, concentrations of Na, K, and Mg were relatively invariant across all wells and similar to their annual averages. Sulfate concentrations were slightly below average in most wells and substantially below average in wells 8 and 14 (Fig. 7). DOC concentrations were consistently lower in subsurface water $(0.6 \pm 0.2 \,\mathrm{mmol}\,\mathrm{L}^{-1})$ than in surface water $(1.6 \pm 0.4 \,\mathrm{mmol}\,\mathrm{L}^{-1})$ along the length of the channel, with the exception of subsurface water in well 8 (1.8 mmol L⁻¹) (Fig. 6). Fe-corrected SUVA₂₅₄ values were higher for subsurface water $(4.3 \pm 1.7 \,\mathrm{Lmg} \cdot \mathrm{C}^{-1} \,\mathrm{m}^{-1})$ than surface water $(2.8 \pm 1.2 \,\mathrm{Lmg} \cdot \mathrm{C}^{-1} \,\mathrm{m}^{-1})$ $C^{-1} m^{-1}$) (Table 3).

Sullivan et al. (2016a) previously reported that annual average concentrations of dissolved oxygen were highest in wells draining the hillslope and the upper stream bed (up to $\sim\!10\,\mbox{mg}\,\mbox{L}^{-1}$) but dipped as low as $1.6\,\pm\,0.3\,\mbox{mg}\,\mbox{L}^{-1}$ near the lithologic boundary (wells 6–8) (Fig. 6). Well water draining the hillslope (well 9) in particular exhibited substantial variation in DO throughout the year, ranging from $\sim\!5$ to $10\,\mbox{mg}\,\mbox{L}^{-1}$. Subsurface water from well 8 also exhibited variable

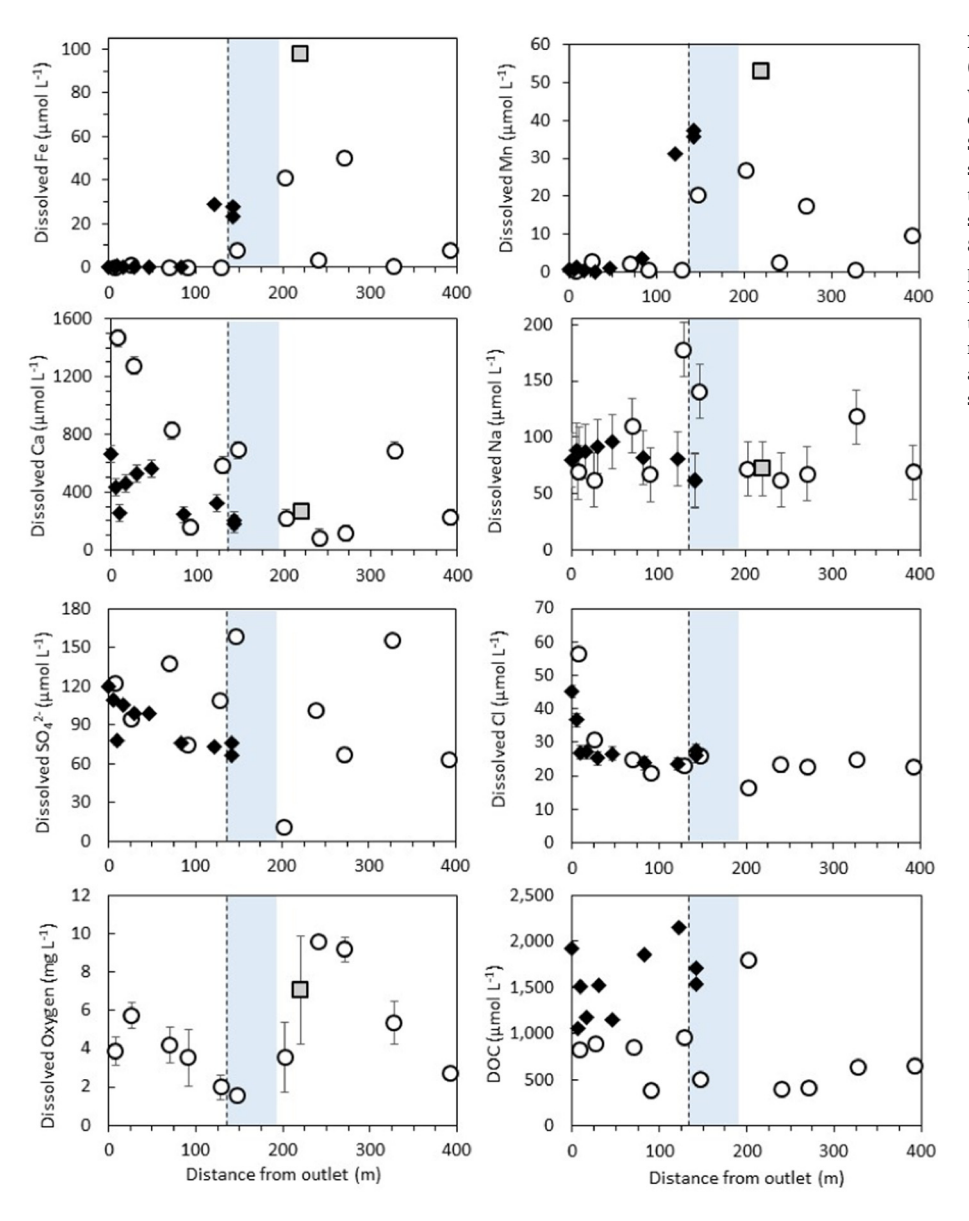


Fig. 6. Concentrations of $<0.45\,\mu m$ filtered solutes $(\mu mol\,L^{-1})$ and dissolved oxygen $(mg\,L^{-1})$ in surface water (filled diamonds) and subsurface water (open circles) collected from SSHCZO in October 2014. Surface water consisted of disconnected pools in the stream bed. The vertical grey bar indicates the potential zone of upwelling from groundwater to the stream bed, defined as the area between wells 6 and 8. The vertical dashed line indicates the approximate position of the lithological boundary shown in Fig. 2. Error bars are equal to the standard error of analytical analysis and are smaller than the symbols where not visible. Well 9, plotted as a grey square, was not analyzed for organic or inorganic anions due to low sample volume.

DO (3.6 $\pm~1.8\,mg\,L^{-1})$ during the year and smelled strongly of H_2S ("rotten-egg smell") at the time of sampling, suggesting transient reducing conditions.

3.3. Element ratios and mixing diagrams

To more directly identify inputs of different water sources to the stream, element ratios (Fe/Na and Mn/Na) in surface water pools were compared to element ratios in subsurface water, and to values reported previously for stream water at low and high flows (Herndon et al., 2015a), and for soil water from planar and swale hillslopes (Herndon et al., 2015b) (Fig. 8). Low and high flow conditions were defined as the lower and upper quartile of discharge values, respectively. Metal concentrations were normalized to Na concentrations to account for changes in water volume due to dilution or evaporative effects. Subsurface water was differentiated as upper well water (collected upstream of the lithologic boundary; wells 7–16) and lower well water (collected downstream of the lithologic boundary; wells 2–6 and 17).

Surface water collected during the dry season varied along the length of the channel: Fe/Na and Mn/Na ratios were high in water collected near the headwaters but lower further downstream. Similarly, well water from the upper catchment was metal-rich while well water

from the lower catchment was relatively metal-poor. Metal concentrations were also high in soil water from swale soils and in perched groundwater draining the swale hillslope (well 9). Metal content was relatively low in soil water from planar soils. Metal contributions from swale soils may even be underestimated in Fig. 8 because the soil water chemistry is averaged across all depths for each site and does not reflect the elevated metal concentrations measured in shallow soil water. For example, Mn concentrations average between 8 and $13\,\mu\mathrm{mol}\,L^{-1}$ (max = $24.3\,\mu\mathrm{mol}\,L^{-1}$) at 10 cm depth in swale soils but never exceed $5\,\mu\mathrm{mol}\,L^{-1}$ below 50 cm depth or in any planar soils (Herndon, 2012; Herndon et al., 2015b). Stream chemistry averaged over low flow conditions was similar to surface and subsurface water in the upper catchment and to soil water from the swale transect.

4. Discussion

We present a conceptual framework in which chemodynamic solute behavior is driven by temporally variable connections between spatially variable source pools. Spatial variability in source pools is driven by biogeochemical processes that concentrate chemodynamic solutes in organic-rich soils. Seasonal variability in flow paths is controlled by catchment structure at the surface, where flow through convergent

Table 3
Water chemistry of surface and subsurface water sampled October 11–12, 2014.

Site ID ^a	Distance ^b	pH	Na+	K ⁺	Ca ²⁺	Mg^{2+}	$Fe_{TOT} \\$	Fe ²⁺	Mn^{2+}	Cl-	SO_4^{2-}	Br ⁻	NO_3^-	PO ₄ ³⁻	DOC
	m		μМ	μΜ	μМ	μΜ	μΜ	μМ	μМ	μМ	μМ	μМ	μΜ	μМ	μΜ
Detection limit			43	26	25	41	0.18	9.0	0.18	3.2	1.2	1.5	1.9	2.5	83
Std. err.			24	31	58	109	0.15	3	0.09	1.15	0.74	0.72	1.43	0.87	60
Stream - T5	0	6.75	80	50	663	237	< DL	n.a.	0.49	45	120	1.6	< DL	< DL	1921
Stream - T1001	6	6.73	89	50	431	293	< DL	n.a.	0.60	37	109	< DL	< DL	< DL	1060
Stream - T11	9	6.76	86	63	254	228	0.65	n.a.	1.24	27	78	< DL	< DL	< DL	1512
Stream - T1030	17	6.78	88	50	456	310	< DL	n.a.	0.41	27	106	< DL	< DL	< DL	1171
Stream - T1032	30	7.40	92	58	529	351	< DL	n.a.	< DL	25	99	2.7	< DL	< DL	1522
Stream - T75	47	6.85	96	64	559	362	0.26	n.a.	1.00	27	99	< DL	< DL	< DL	1146
Stream - T1101	83	6.80	82	55	242	228	0.30	n.a.	3.34	24	76	< DL	< DL	< DL	1859
Stream - T259	122	6.82	81	50	322	270	29.0	n.a.	31.2	24	73	< DL	< DL	< DL	2153
Stream - T1213	142	6.65	62	67	206	174	23.4	n.a.	37.4	28	67	< DL	< DL	< DL	1714
Stream - T1213 (2)	142	6.37	61	59	180	149	27.8	n.a.	35.8	26	76	< DL	< DL	< DL	1538
SSHCZO Well 17	8	7.07	69	12	1465	198	< DL	< DL	< DL	57	122	1.6	11.3	< DL	827
SSHCZO Well 2	26	6.74	62	< DL	1276	44	0.75	< DL	2.70	31	94	< DL	4.5	< DL	885
SSHCZO Well 4	70	7.04	110	26	827	473	< DL	< DL	1.97	25	137	1.5	5.0	< DL	849
SSHCZO Well 5	91	5.62	67	< DL	155	56	< DL	< DL	0.28	21	74	< DL	15.0	< DL	376
SSHCZO Well 6	129	7.13	178	28	586	336	< DL	< DL	0.40	23	109	< DL	25.3	< DL	953
SSHCZO Well 7	147	7.46	140	< DL	690	498	7.59	7.50	20.4	26	158	1.6	< DL	< DL	508
SSHCZO Well 8	202	6.76	72	29	218	180	40.9	49.8	26.6	16	11	< DL	< DL	8.52	1804
SSHCZO Well 10	240	5.72	62	31	83	80	3.02	< DL	2.21	23	101	< DL	13.1	< DL	391
SSHCZO Well 11	271	6.52	67	< DL	113	99	50.2	62.4	17.5	23	67	< DL	3.0	< DL	412
SSHCZO Well 13	327	6.72	118	38	689	693	0.29	< DL	0.25	25	156	< DL	3.9	< DL	642
SSHCZO Well 14	392	n.a.	69	39	224	329	7.61	10.3	9.67	23	64	< DL	< DL	17.21	643
SSHCZO Well 9	220	6.37	72	47	267	195	97.6	102	53.0	n.a.	n.a.	n.a.	n.a.	n.a.	n.a.c

^a Stream ID refers to identification number of tree located closest to the sampling site.

hillslopes persists through the dry season, and in the subsurface, where lithology dictates groundwater flow and mixing.

4.1. Element mobilization from soils and sediments

Shallow soils that are sources of dissolved organic carbon released high concentrations of mobile elements into solution as either dissolved ions (e.g., Mn, Ca, Al) or colloids and particles (e.g., Fe, P, Al, Ti) (Fig. 3). Deeper soils released lower amounts of these elements in their mobile forms. These results indicate that both metals and base cations were more easily mobilized from organic-rich surface soils. This pattern can be explained by differences in weathering environments as well as the abundance and chemical form of each element as a function of soil depth.

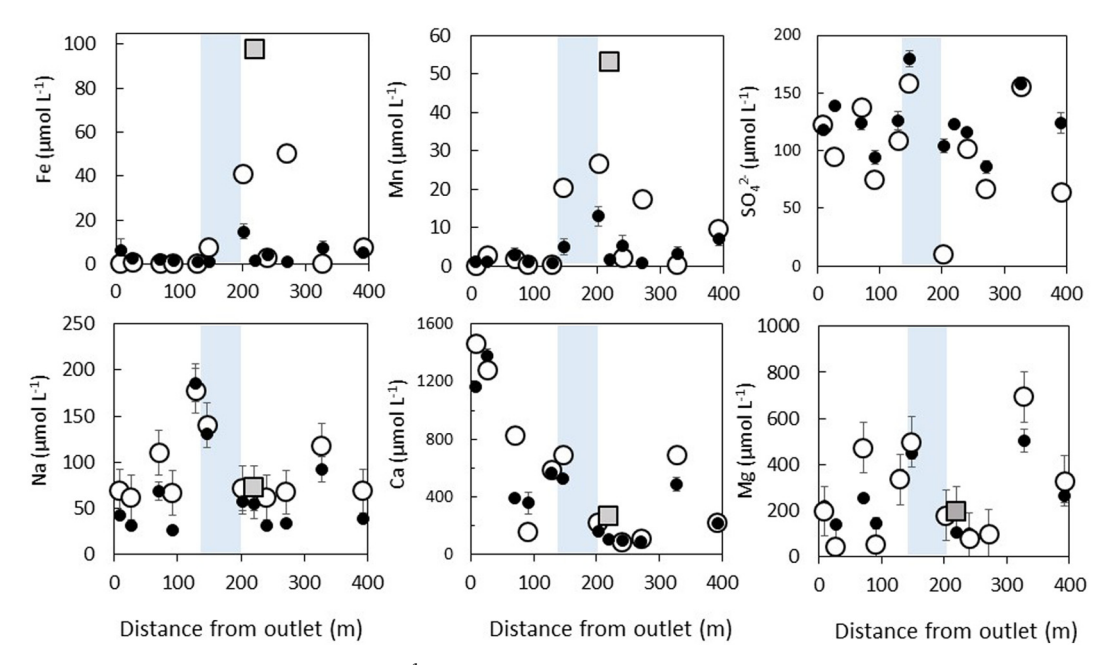


Fig. 7. Concentrations of $< 0.45 \,\mu m$ filtered elements ($\mu mol \, L^{-1}$) in subsurface water analyzed in this study (open symbols) and averaged over the year (closed symbols; Sullivan et al., 2016a) as a function of distance from the catchment outlet (m). The vertical shaded bar indicates the potential zone of upwelling between wells 6 and 8 and denotes a transition from the lower, western part of the catchment and upper, eastern part of the catchment. Error bars represent analytical error for open symbols and standard deviation for closed symbols and are smaller than the symbol where not visible. The hillslope well (well 9) is plotted as a grey square.

^b Distance from the catchment outlet (weir) along the stream bed.

^c n.a. values indicate that analyte was not measured for that sample.

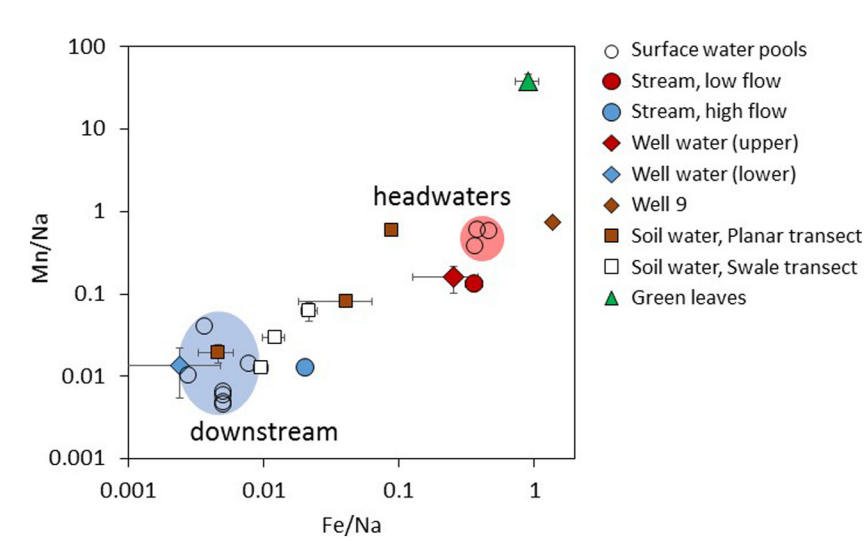


Fig. 8. Log-log plot of Fe/Na and Mn/Na ratios in $< 0.45 \, \mu m$ filtered surface water (circles), subsurface water (diamonds), and soil water (squares). Element ratios for whole green leaves (triangle) are shown for comparison as an organic-rich endmember. Surface, subsurface, and soil water are further differentiated by symbol color. Surface water includes stream water exiting the catchment at 1) low flow (closed red circle) or 2) high flow (closed blue circle) conditions, and stream water sampled from standing pools at 3) the headwaters (122-142 m from outlet; open circles with red overlay) or 4) downstream (≤83 m from outlet; open circles with blue overlay) during no flow conditions. Three chemically distinct types of subsurface water were also identified as well water draining: 1) the upper portion of the catchment (red diamond), 2) the lower portion of the catchment (blue diamond), and 3) a swale hillslope (brown diamond). Finally, the chemical composition of soil water along a planar hillslope (open squares) was chemically distinct from soil water along a proximal swale hillslope (brown squares). Stream water composition under low flow conditions is chemically similar to that of swale water (soil and well 9) and water from the

headwaters of the catchment (both subsurface and surface water). Conversely, stream water composition under high flow conditions is similar to planar soil water and water from the downstream portion of the catchment (both groundwater and surface water pools). Error bars are equal to the standard error of the mean. Soil water chemistry represents solute concentrations averaged across all depths for ridge top, midslope, and valley floor soils located in parallel planar and swale hillslopes on the south slope, as reported by Herndon et al. (2015b). (For interpretation of the references to color in this figure legend, the reader is referred to the web version of this article.)

Manganese, Ca, and P are concentrated in surface soils at the SSHCZO, partially due to biological cycling that accumulates these elements in leaves and returns them to the soil in leaf litter (Herndon et al., 2015b), and partially due to atmospheric deposition (Herndon et al., 2011; Meek et al., 2016). High concentrations of dissolved P, Ca, and Mn extracted from shallow soils are attributed to HPO₄²⁻, Ca²⁺, and Mn2+ ions that are liberated from organic matter during decomposition and temporarily retained as exchangeable ions prior to leaching (Jin et al., 2010; Herndon et al., 2015b). The formation of biogenic Mn-oxides during litter decomposition (Herndon et al., 2014) may contribute to the high proportion of colloidal Mn in shallow soils, as also observed by Bern and Yesavage (2018). Colloidal P in shallow soils could derive from P contained in organic matter or phosphate that is sorbed to colloidal Fe and Al oxides (Stewart and Tiessen, 1987; Henderson et al., 2012). Deeper soils released concentrations of colloidal P that were similar to the shale bedrock and may indicate mobilization of a P-bearing primary mineral.

Increased mobility of Fe and Al species in shallow soils may be explained by mineral weathering that produces secondary minerals and dissolved species. Iron oxides and Al-bearing kaolinite accumulate in shallow soils following dissolution of primary illite and chlorite (Jin et al., 2010). High concentrations of dissolved Al3+ extracted from shallow soils are attributed to Al³⁺ ions that are released from mineral weathering and stored as exchangeable cations. Previous studies proposed that Fe and Al are primarily lost as fine particles from soils that develop on planar hillslopes (Jin et al., 2010; Yesavage et al., 2012; Sullivan et al., 2016b). Given that the planar soils examined here contained very low concentrations of dissolved or colloidal Fe, similar to reports by Bern and Yesavage (2018), we infer that Fe was preferentially mobilized as micron-sized particles of iron oxides (Fig. 5a). In contrast, Al was mobilized both as small particles of kaolinite (Fig. 5a) and as dissolved and colloidal phases (Fig. 3). Colloidal Al may consist of aluminum oxides produced during kaolinite weathering. Although Fe and Al are highly insoluble in oxic soil environments, complexation by organic molecules could increase Fe and Al solubility (Neaman et al., 2006). Titanium was only mobilized in micron-sized particles (Fig. 5a), which supports Ti depletion from soils due to particle loss rather than leaching.

The high proportion of colloidal metals identified in this study are consistent with previous findings that most metals exhibit moderate to strong colloidal influence (Trostle et al., 2016). Indeed, Bern and

Yesavage (2018) found that colloid mobilization exceeded solute leaching for all elements in planar soils at SSHCZO. Although our measurements indicate that solutes comprise a larger portion of mobile elements, this discrepancy can be explained by differences in the size fraction of colloids examined by each study. Bern and Yesavage (2018) report that colloids were dominated by micron-sized clay minerals, which were excluded from the colloid fraction defined in this study but visually identified in the particulate fraction (Fig. 5a). Exclusion of colloidal clay from our analysis would increase the relative proportion of elements in the dissolved phase.

The planar soils examined in this study may even underestimate the magnitude of elements mobilized from swale soils. Previous studies at the SSHCZO have found that soils and pore waters on swale hillslopes are chemically different from those on planar hillslopes (Andrews et al., 2011; Herndon et al., 2015b). For example, pore waters collected from swale hillslopes contain higher concentrations of DOC and soluble metals than pore waters collected from planar hillslopes (Fig. 8). The organic-rich shallow soils (0–10 cm) examined here represent the best approximation for soils contained in swale hillslopes.

4.2. Hydrologic connectivity drives concentration-discharge behavior

Our results support the conceptual model in which the intermittent stream in the SSHCZO headwaters catchment receives inputs primarily from hillslopes and shallow interflow rather than from regional groundwater (Fig. 9) (Sullivan et al., 2016a; Li et al., 2017). Consequently, chemodynamic solute concentrations in the stream vary with discharge due to spatial and temporal variability in element delivery from hillslope soils to the stream channel. The water table remained over a meter below the stream channel except at a lithologic boundary near the stream headwaters where upwelling water was metal-rich, similar to soil water from swale soils and to water draining a swale on the north slope (well 9) (Fig. 8). These results indicate that chemodynamic metals (Fe, Mn) are mobilized from organic-rich soils in swales and transported along fast flow paths (e.g., macropores) to the fractured zone below the soil. Yesavage et al. (2012) previously identified that similar macropore flow delivered particulate Fe directly from soils to stream when the catchment was saturated. Consistent with recent hillslope hydrologic models (Brantley et al., 2017), we infer that flow was predominantly vertical within the soil zone and lateral in the fractured zone beneath the soil during dry periods. Interflow that moves

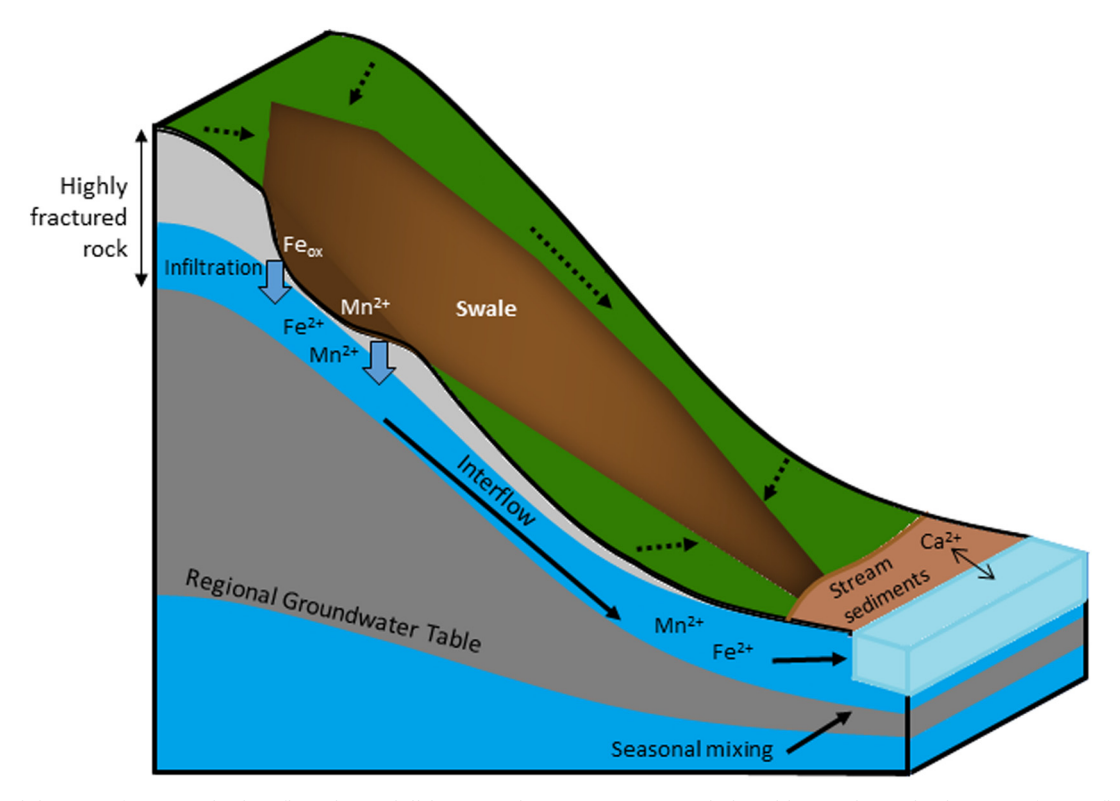


Fig. 9. Conceptual diagram of water and solute flow along a hillslope into the stream. Arrows with dotted lines indicate the direction of water flow through soils along planar hillslopes (shown in green) and into convergent swale regions (shown in brown). Solid arrows indicate subsurface water flow paths that include both regional groundwater and interflow, a shallow perched water table that drains soils and flows through a highly fractured zone towards the stream. During the dry season, interflow receives inputs primarily from swales, and regional groundwater is disconnected from the stream. Chemical species indicate mobilization of chemodynamic elements from either swales (Fe and Mn) or stream sediments (Ca). Iron is mobilized as iron oxide particles (Fe $_{ox}$) but undergoes reductive dissolution in the subsurface to generate dissolved Fe $^{2+}$. Diagram is not to scale. (For interpretation of the references to color in this figure legend, the reader is referred to the web version of this article.)

through the fractured regolith supplies the stream with water during the dry season when planar soils and the regional water table remain disconnected from the stream. Surface water further downstream was relatively metal-poor (Fig. 6) and chemically similar to subsurface water in the lower catchment (Fig. 8). Since the water table was well below the land surface near these pools, this suggests the downstream pools were recharged either by interflow through planar hillslope soils or by groundwater that rose to the stream bed during rain events and became isolated as the water table dropped. Alternatively, if regional groundwater was able to reach the surface through undocumented fractures, lack of stream flow in the dry season could be explained by high rates of evaporation that exceeded inputs from the subsurface.

Sullivan et al. (2016a) proposed that young shallow interflow, represented by water from well 8, mixes with older regional groundwater just upslope of well 7. High concentrations of dissolved oxygen in the interflow drive pyrite oxidation, consuming oxygen and generating sulfate (Jin et al., 2014). Indeed, well 7 was enriched in dissolved SO_4^{2-} , Ca, Mg, and Na but depleted in Fe, Mn, and DOC relative to well 8 (Fig. 6). These patterns support the idea that shallow interflow comprises subsurface water in the eastern part of the catchment and mixes seasonally with base-cation enriched regional groundwater near the lithologic boundary. The change in lithology is important because low permeability shale in the eastern portion of the catchment generates the perched water table that delivers flow to the channel. Higher permeability sandstones in the western portion facilitate deeper infiltration to the regional water table.

High concentrations of dissolved metals coupled with low concentrations of sulfate in eastern wells denote reducing conditions that may result from depletion of dissolved oxygen during dry months. Well 8 in particular was depleted in sulfate, and $\rm H_2S$ production was inferred

by the presence of a rotten egg smell during sampling. In comparison, concentrations of the relatively conservative element Na were similar to annual averages, indicating that changes in redox condition rather than water source was responsible for the change in interflow chemistry. Exceptionally high concentrations of DOC in well 8 support the idea that metals are sourced from organic-rich soils rather than from dissolution of deeper ankerite layers (Jin et al., 2014). Subsurface water was also depleted in DOC but enriched in aromatic-C relative to surface water and soil water (Fig. 4), suggesting that non-aromatic C was removed by biodegradation during infiltration into the subsurface. Microbial oxidation of labile organic compounds would consume dissolved oxygen and promote reducing conditions.

The stream headwaters, located near the zone of upwelling, were chemically similar to interflow from well 8 but with higher concentrations of ${\rm SO_4}^{2-}$ and lower dissolved Fe. These patterns can be attributed to sulfide and ferrous iron oxidation, respectively. Ferrous iron oxidation would lower concentrations of dissolved Fe as iron oxyhydroxides precipitate out of solution. It is unlikely that regional groundwater contributes to the stream headwaters given that the headwaters do not contain elevated concentrations of weathering products (Ca, Mg, Na) that characterize groundwater. Rather, concentrations of these elements increase downstream while concentrations of Fe and Mn decrease. We propose that interflow infiltrating swale regions recharges the headwaters during periods of intermittent flow as observed in this study. During wetter periods of continuous stream flow, interflow is increasingly derived from soil water that infiltrates relatively organic-poor soils on planar hillslopes. As the water table rises during high discharge events, regional groundwater, containing low dissolved metals, may contribute to stream flow in the downslope portion of the catchment (Fig. 8). These shifting hydrologic connections

can explain why chemodynamic elements that are concentrated in swales (Fe, Mn) become diluted in the stream with increasing discharge.

Dissolved Ca in the stream exhibits dilution behavior similar to Fe and Mn; however, inputs of interflow from swales cannot explain high concentrations of stream Ca at low discharge. Opposite to the trends observed for Fe and Mn, Ca concentrations in both surface and subsurface water are low in the upper catchment and increase towards the outlet (Fig. 6) due to increasing contributions from carbonate weathering (Jin et al., 2011; Jin et al., 2014; Meek et al., 2016). However, inputs of carbonate-influenced groundwater cannot explain high Ca concentrations at low discharge because groundwater only contributes to the stream during high flow. High concentrations of Ca at low flow are better explained by inputs of exchangeable Ca from the stream sediments. Stream sediments contain high concentrations of water-soluble Ca^{2+} (1760 ± 620 µmol kg⁻¹; n = 2) relative to $(120 \pm 50 \,\mu\text{mol kg}^{-1}; n = 11)$ (Fig. 3; Table 1). This Ca²⁺ is likely derived from dissolution of secondary calcite that precipitates in the shallow fractured zone below the stream bed (Kuntz et al., 2011; Brantley et al., 2013; Jin et al., 2014; Sullivan et al., 2016a). During wet periods, groundwater contributions to the stream increase and enrich stream sediments and valley floor soils with Ca²⁺ that is retained on exchange sites (Meek et al., 2016). A similar mechanism was proposed by Hoagland et al. (2017) for a nearby sandstone catchment. Hoagland et al. (2017) attributed Ca concentration-discharge behavior to varying inputs from the hyporheic zone, where high concentrations of exchangeable Ca were stored in sediments. Exchangeable Ca was derived from carbonate-rich groundwater that periodically replenished the hyporheic zone with Ca when the water table rose.

Calcite is a more likely source of Ca than deep carbonates (Jin et al., 2010) given that carbonates contain Mg that should exhibit similar trends to Ca. However, Mg displays chemostatic behavior that is attributed to clay rather than carbonate dissolution (Li et al., 2017). Furthermore, stream ratios of Mg/Na are similar between high flow (3.7 \pm 0.2) and low flow (4.2 \pm 0.1) while Ca/Na increases from 6.3 \pm 0.3 at high flow to 11.5 \pm 0.4 at low flow (Herndon et al., 2015a), indicating input of a source that contains high Ca but not Mg or Na

To summarize, high concentrations of chemodynamic solutes at low discharge are explained by the dominance of interflow from organic-rich swales and cation exchange with stream sediments. Chemodynamic solutes are diluted at high discharge as flow through planar hillslopes, and regional groundwater to a lesser extent, contribute a higher proportion of stream flow. Chemostatic solutes do not exhibit dilution behavior because soil solute concentrations are relatively homogeneous throughout the catchment.

4.3. Geochemical transformations along flow paths

Iron was mobilized from soils primarily in colloids and particles that presumably contained iron (III) oxyhydroxides, but enriched in shallow interflow as dissolved Fe²⁺. Anoxic conditions can promote metal oxide reduction and increase concentrations of dissolved metals in groundwater; however, concentrations of dissolved metals were not correlated with average concentrations of dissolved oxygen (p > 0.05). Rather, concentrations of dissolved Mn and Fe were high in wells with highly variable DO concentrations, from < 2 to $10 \,\mathrm{mg}\,\mathrm{L}^{-1}$. The observed pattern is more consistent with oxygenated, metal-rich water draining the hillslopes. Colloidal and particulate iron oxides then experience reductive dissolution coupled to oxidation of organic matter in the subsurface. Indeed, concentrations of dissolved metals were high in pore waters of organic-rich soils such as the swale soils that overly the hillslope well (9) (Fig. 8). Swales and the stream bed retain more moisture throughout the year than planar hillslope soils and disproportionately contribute to interflow during dry months (Lin et al., 2006; Qu and Duffy, 2007; Bao et al., 2017; Li et al., 2017). Low DO

concentrations observed in subsurface water could be due to stagnation of interflow. That is, metal and organic-rich infiltrating water collects and flows slowly through a depression, e.g., at the contact boundary, and is not quickly replenished during the dry period, leading to microbial reduction of oxidized species.

The potential for metal oxides to precipitate out of upwelling interflow was observed during artificial oxidation of well water. Metalrich interflow obtained from well 8 developed Fe- and Mn-rich precipitates following collection and filtration (Fig. 5b). Oxidation of upwelling interflow may at least partially explain the presence of particulate Fe in stream water at Shale Hills (Yesavage et al., 2012), while seasonal oxidation of interflow in the subsurface may contribute to Fe oxide precipitation along fracture zones (Kuntz et al., 2011). Oxidation of upwelling interflow can also explain decreasing concentrations of dissolved Fe in stream headwaters relative to interflow but high concentrations of colloidal Fe in stream sediments. High concentrations of colloidal Fe in stream sediments are consistent with high concentrations of acid-soluble Fe, a proxy for poorly crystalline iron oxides, reported by Yesavage et al. (2012). Although colloidal Fe could still be transported in the stream and measured in < 0.45 µm filtrate, colloid aggregation or association with larger particles would remove Fe from solution. Thus, temporal variability in Fe oxidation and removal could contribute to the observed dilution trend but was not investigated in this study.

Iron and Mn-rich precipitates collected from oxygenated interflow contained high concentrations of C and P, suggesting co-precipitation of organic matter and/or phosphate adsorption (Zak et al., 2004; Riedel et al., 2013). Consequently, sediments may serve as a temporary sink for metal oxides that sequester small quantities of C and P, although the extent to which this process controls nutrient processing in the stream remains unknown.

5. Conclusions

The purpose of this study was to elucidate how temporal and spatial heterogeneity regulate concentration-discharge behavior in a headwater catchment. We examined how elements are mobilized from hillslope soils and transported along subsurface flow paths to the stream. We also investigated the spatial variability of surface and subsurface hydrochemistry at low flow in order to identify surface-subsurface interactions that may have been obscured during higher flow conditions. In particular, we focused on chemodynamic elements (Fe, Mn, Ca) that exhibited dilution behavior; that is, concentrations were high in the stream at low flow but quickly diluted as flow increased

Surface water was disconnected from subsurface water along the length of the channel during the dry period, except in an upwelling zone near a lithological transition from shale to sandstone-interbedded shale. Stream headwaters at the lithologic boundary consisted of upwelling, shallow interflow that delivered Fe and Mn-rich water derived from convergent hillslopes laterally though a subsurface fracture zone and into the stream channel (Fig. 9). We propose that dilution behavior at the stream outlet reflects changes in hydrologic connectivity of hillslopes to the stream with increasing discharge. During dry periods when the stream is confined to disconnected pools and discharge is low, rainfall events flush Fe and Mn-rich headwaters derived from shallow interflow to the stream outlet. High concentrations of Ca cannot be explained by export from swales and are instead attributed to mobilization of exchangeable Ca stored in stream sediments and soils on the valley floor. As discharge increases with more intense rainfall and during wetter periods when stream flow is established, chemodynamic elements are diluted by increased inputs from metal-poor hillslope soils and lesser contributions from the regional groundwater table.

This study highlights how catchment structure defines spatial variability in source pools and temporal variability in flow paths that control the concentration-discharge behavior of chemodynamic

elements. The intermittent and ephemeral streams that comprise the majority of headwater catchments may be particularly sensitive to dynamic hydrologic connectivity, as observed at the Shale Hills CZO. Thus, complex interactions between geology, hydrology, and biogeochemistry are important to consider when modeling chemical export from headwater catchments.

Supplementary data to this article can be found online at https://doi.org/10.1016/j.chemgeo.2018.06.019.

Acknowledgements

Research was supported by subaward 5058-KSU-NSF-1726 (E. Herndon) from NSF EAR-1331726 (S. Brantley) for the Susquehanna Shale Hills Critical Zone Observatory. Logistical support and/or data were provided by the NSF-supported Susquehanna Shale Hills Critical Zone Observatory. This research was conducted in Penn State's Stone Valley Forest, which is funded by the Penn State College of Agriculture Sciences, Department of Ecosystem Science and Management and managed by the staff of the Forestlands Management Office. The Fall 2014 Hydrogeochemistry class in the Department of Geology at Kent State University is acknowledged for surface and groundwater collection and analysis.

References

- Aiken, G.R., Hsu-Kim, H., Ryan, J.N., 2011. Influence of dissolved organic matter on the environmental fate of metals, nanoparticles, and colloids. Environ. Sci. Technol. 45, 3196–3201.
- Ameli, A.A., Beven, K., Erlandsson, M., Creed, I.F., McDonnell, J.J., Bishop, K., 2017.Primary weathering rates, water transit times, and concentration-discharge relations:a theoretical analysis for the critical zone. Water Resour. Res. 942–960.
- Andrews, D.M., Lin, H., Zhu, Q., Jin, L., Brantley, S.L., 2011. Hot spots and hot moments of dissolved organic carbon export and soil organic carbon storage in the Shale Hills catchment. Vadose Zone J. 10, 943.
- Bao, C., Li, L., Shi, Y., Duffy, C., 2017. Understanding watershed hydrogeochemistry: 1. Development of RT-flux-PIHM. Water Resour. Res. 53, 2328–2345.
- Baronas, J.J., Torres, M.A., Clark, K.E., West, A.J., 2017. Mixing as a driver of temporal variations in river hydrochemistry: 2. Major and trace element concentration dynamics in the Andes-Amazon transition. Water Resour. Res. 53, 3120–3145.
- Bern, C., Yesavage, T., 2018. Geochemical modeling of small mineral particle losses from sedimentary rock-derived soils. Geochim. Cosmochim. Acta 476, 441–455.
- Bern, C.R., Thompson, A., Chadwick, O.A., 2015. Quantification of colloidal and aqueous element transfer in soils: the dual-phase mass balance model. Geochim. Cosmochim. Acta 151, 1–15. http://dx.doi.org/10.1016/j.gca.2014.12.008.
- Bishop, K., Seibert, J., Köhler, S., Laudon, H., 2004. Resolving the double paradox of rapidly mobilized old water highly variable responses in runoff chemistry. Hydrol. Process. 18, 185–189.
- Brantley, S.L., Holleran, M.E., Jin, L., Bazilevskaya, E., 2013. Probing deep weathering in the Shale Hills critical zone observatory, Pennsylvania (USA): the hypothesis of nested chemical reaction fronts in the subsurface. Earth Surf. Process. Landf. 38, 1280–1298.
- Brantley, S.L., Lebedeva, M.I., Balashov, V.N., Singha, K., Sullivan, P.L., Stinchcomb, G., 2017. Toward a conceptual model relating chemical reaction fronts to water flow paths in hills. Geomorphology 277, 100–117.

 Ghani, A., Dexter, M., Perrott, K.W., 2003. Hot-water extractable carbon in soils: a sen-
- Ghani, A., Dexter, M., Perrott, K.W., 2003. Hot-water extractable carbon in soils: a sensitive measurement for determining impacts of fertilisation, grazing and cultivation. Soil Biol. Biochem. 35, 1231–1243.
- Godsey, S.E., Kirchner, J.W., Clow, D.W., 2009. Concentration-discharge relationships reflect chemostatic characteristics of US catchments. Hydrol. Process. 23, 1844–1864.
- Henderson, R., Kabengi, N., Mantripragada, N., Cabrera, M., Hassan, S., Thompson, A., 2012. Anoxia-induced release of colloid- and nanoparticle-bound phosphorus in grassland soils. Environ. Sci. Technol. 46, 11727–11734.
- Herndon, E., 2012. Biogeochemistry of Manganese Contamination in a Temperate Forested Watershed. The Pennsylvania State University.
- Herndon, E.M., Jin, L., Brantley, S.L., 2011. Soils reveal widespread manganese enrichment from industrial inputs. Environ. Sci. Technol. 45, 241–247.
- Herndon, E.M., Martínez, C.E., Brantley, S.L., 2014. Spectroscopic (XANES/XRF) characterization of contaminant manganese cycling in a temperate watershed. Biogeochemistry 121 (3), 505–517.
- Herndon, E.M., Dere, A.L., Sullivan, P.L., Norris, D., Reynolds, B., Brantley, S.L., 2015a. Landscape heterogeneity drives contrasting concentration-discharge relationships in shale headwater catchments. Hydrol. Earth Syst. Sci. 19, 3333–3347.
- Herndon, E.M., Jin, L., Andrews, D.M., Eissenstat, D.M., Brantley, S.L., 2015b. Importance of vegetation for manganese cycling in temperate forested watersheds. Glob. Biogeochem. Cycles 29, 160–174.
- Hoagland, B., Russo, T.A., Gu, X., Hill, L., Kaye, J., Forsythe, B., Brantley, S.L., 2017. Hyporheic zone influences on concentration-discharge relationships in a headwater sandstone stream. Water Resour. Res. 53 (6), 4643–4667.
- Jin, L., Ravella, R., Ketchum, B., Bierman, P.R., Heaney, P., White, T., Brantley, S.L.,

- 2010. Mineral weathering and elemental transport during hillslope evolution at the Susquehanna/Shale Hills critical zone observatory. Geochim. Cosmochim. Acta 74, 3669–3691. http://dx.doi.org/10.1016/j.gca.2010.03.036.
- Jin, L., Andrews, D.M., Holmes, G.H., Lin, H., Brantley, S.L., 2011. Opening the "black box": water chemistry reveals hydrological controls on weathering in the Susquehanna Shale Hills critical zone observatory. Vadose Zone J. 10, 928–942.
- Jin, L., Ogrinc, N., Yesavage, T., Hasenmueller, E.A., Ma, L., Sullivan, P.L., Kaye, J., Duffy, C., Brantley, S.L., 2014. The CO₂ consumption potential during gray shale weathering: insights from the evolution of carbon isotopes in the Susquehanna Shale Hills critical zone observatory. Geochim. Cosmochim. Acta 142, 260–280. http://dx.doi.org/10.1016/j.gca.2014.07.006.
- Johnson, N.M., Likens, G.E., Bormann, F.H., Fisher, D.W., Pierce, R.S., 1969. A working model for the variation in stream water chemistry at the Hubbard Brook Experimental Forest, New Hampshire. Water Resour. Res. 5, 1353–1363.
- Kim, H., Dietrich, W.E., Thurnhoffer, B.M., Bishop, J.K.B., Fung, I.Y., 2017. Controls on solute concentration-discharge relationships revealed by simultaneous hydrochemistry observations of hillslope runoff and streamflow: the importance of critical zone structure. Water Resour. Res. 53 (2), 1424–1443.
- Kirchner, J.W., 2003. A double paradox in catchment hydrology and geochemistry. Hydrol. Process. 17, 871–874. Available at. https://doi.org/10.1002/hyp.5108.
- Kraepiel, A.M.L., Dere, A.L., Herndon, E.M., Brantley, S.L., 2015. Natural and anthropogenic processes contributing to metal enrichment in surface soils of central Pennsylvania. Biogeochemistry 123, 265–283.
- Kuntz, B.W., Rubin, S., Berkowitz, B., Singha, K., 2011. Quantifying solute transport at the Shale Hills critical zone observatory. Vadose Zone J. 10, 843.
 Li, L., Bao, C., Sullivan, P.L., Brantley, S., Shi, Y., Duffy, C., 2017. Understanding wa-
- Li, L., Bao, C., Sullivan, P.L., Brantley, S., Shi, Y., Duffy, C., 2017. Understanding watershed hydrogeochemistry: 2. Synchronized hydrological and geochemical processes drive stream chemostatic behavior. Water Resour. Res. 53, 2346–2367.
- Lin, H.S., Kogelmann, W., Walker, C., Bruns, M.A., 2006. Soil moisture patterns in a forested catchment: a hydropedological perspective. Geoderma 131, 345–368.
- Ma, L., Konter, J., Herndon, E., Jin, L., Steinhoefel, G., Sanchez, D., Brantley, S., 2014.Quantifying an early signature of the industrial revolution from lead concentrations and isotopes in soils of Pennsylvania, USA. Anthropocene 7, 16–29.
- Maher, K., 2011. The role of fluid residence time and topographic scales in determining chemical fluxes from landscapes. Earth Planet. Sci. Lett. 312, 48–58.
- McIntosh, J.C., Schaumberg, C., Perdrial, J., Harpold, A., Vazquez-Ortega, A., Rasmussen, C., Vinson, D., Zapata-Rios, X., Brooks, P.D., Meixner, T., Pelletier, J., Derry, L., Chorover, J., 2017. Geochemical evolution of the critical zone across variable time scales informs concentration-discharge relationships: Jemez River basin critical zone observatory. Water Resour. Res. 53, 4169–4196.
- Meek, K., Derry, L., Sparks, J., Cathles, L., 2016. ⁸⁷Sr, ⁸⁶Sr, Ca/Sr, and Ge/Si ratios as tracers of solute sources and biogeochemical cycling at a temperate forested shale catchment, central Pennsylvania, USA. Chem. Geol. 445, 84–102.
- Moatar, F., Abbott, B.W., Minaudo, C., Curie, F., Pinay, G., 2017. Elemental properties, hydrology, and biology interact to shape concentration-discharge curves for carbon, nutrients, sediment, and major ions. Water Resour. Res. 53, 1270–1287.
- Nadeau, T.L., Rains, M.C., 2007. Hydrological connectivity between headwater streams and downstream waters: how science can inform policy. J. Am. Water Resour. Assoc. 43, 118–133.
- Neaman, A., Chorover, J., Brantley, S.L., 2006. Effects of organic ligands on granite dissolution in batch experiments at pH 6. Am. J. Sci. 306, 451–473.
- NOAA, 2017. Station Data, USC00368449. Available at: https://www.ncdc.noaa.gov/cdo-web/datasets/GHCND/stations/GHCND:USC00368449/detail, Accessed date: 12 February 2017.
- Qu, Y., Duffy, C.J., 2007. A semidiscrete finite volume formulation for multiprocess watershed simulation. Water Resour. Res. 43.
- Riedel, T., Zak, D., Biester, H., Dittmar, T., 2013. Iron traps terrestrially derived dissolved organic matter at redox interfaces. Proc. Natl. Acad. Sci. 110, 10101–10105.
- Stewart, J.W.B., Tiessen, H., 1987. Dynamics of soil organic phosphorus. Biogeochemistry 4, 41–60.
- Sullivan, P.L., Hynek, S.A., Gu, X., Singha, K., White, T., West, N., Kim, H., Clarke, B., Kirby, E., Duffy, C., Brantley, S.L., 2016a. Oxidative dissolution under the channel leads geomorphological evolution at the shale hills catchment. Am. J. Sci. 316, 981–1026.
- Sullivan, P.L., Ma, L., West, N., Jin, L., Karwan, D.L., Noireaux, J., ... Derry, L.A., 2016b. CZ-tope at Susquehanna Shale Hills CZO: synthesizing multiple isotope proxies to elucidate critical zone processes across timescales in a temperate forested landscape. Chem. Geol. 445, 103–119.
- Torres, M.A., Baronas, J.J., Clark, K.E., Feakins, S.J., West, A.J., 2017. Mixing as a driver of temporal variations in river hydrochemistry: 1. Insights from conservative tracers in the Andes-Amazon transition. Water Resour. Res. 53 (4), 3102–3119.
- Trostle, K.D., Runyon, J.R., Pohlmann, M.A., Redfield, S.E., Pelletier, J., McIntosh, J., Chorover, J., 2016. Colloids and organic matter complexation control trace metal concentration-discharge relationships in Marshall Gulch stream waters. Water Resour. Res. 52 (10), 7931–7944.
- Weishaar, J., Aiken, G., Bergamaschi, B., Fram, M., Fujii, R., Mopper, K., 2003. Evaluation of specific ultra-violet absorbance as an indicator of the chemical content of dissolved organic carbon. Environ. Sci. Technol. 37, 4702–4708.
- Yesavage, T., Fantle, M.S., Vervoort, J., Mathur, R., Jin, L., Liermann, L.J., Brantley, S.L., 2012. Fe cycling in the Shale Hills critical zone observatory, Pennsylvania: an analysis of biogeochemical weathering and Fe isotope fractionation. Geochim. Cosmochim. Acta 99, 18–38. http://dx.doi.org/10.1016/j.gca.2012.09.029.
- Zak, D., Gelbrecht, J., Steinberg, C.E.W., 2004. Phosphorus retention at the redox interface of peatlands adjacent to surface waters in Northeast Germany. Biogeochemistry 70, 357–368.
- Zhang, Q., 2017. Synthesis of nutrient and sediment export patterns in the Chesapeake Bay watershed: complex and non-stationary concentration-discharge relationships. Sci. Total Environ. 618, 1268–1283.